Reactive nitrogen partitioning fuels contribution of Canadian wildfire plumes to U.S. ozone air quality

Meiyun Lin[1*], Larry W. Horowitz[1], Lu Hu[2], Wade Permar[2]

[1] NOAA Geophysical Fluid Dynamics Laboratory, Princeton, NJ, USA
[2] Department of Chemistry and Biochemistry, University of Montana, Missoula, MT, USA

*Corresponding author: Meiyun Lin (Meiyun.Lin@noaa.gov)

Submitted to AGU GRL (12 Publication Unit: 6 Figures, ~3200 words), March 18, 2024

Key Points (140 characters including spaces):

1) Sequestration of NO_x emissions to PAN in fresh Canadian wildfire plumes allows for their downwind impacts on US O_3 air quality.
2) PAN decomposition to NO_x fuels the contribution of O_3 from aged Canadian smoke plumes to cities in Washington, Utah, Colorado and Texas.
3) Accounting for this effect in a variable-resolution global chemistry-climate model enhances smoke-influenced O_3 events in US cities.

Abstract (150 words). Accurately quantifying wildfire impacts on ozone air quality is challenging due to complex physical and chemical processes in wildfire smoke. Here we use measurements from the 2018 WE-CAN aircraft campaign to parameterize emissions of reactive nitrogen (NO_y) from wildfires into PAN (37%), NO_3^- (27%), and NO (36%) in a global chemistry-climate model with 13 km horizontal resolution over the contiguous US. The NO_y partitioning, compared with emitting all NO_y as NO, reduces model ozone bias in near-fire smoke plumes sampled by the aircraft but significantly enhances ozone downwind when Canadian smoke plumes reach cities in Washington state, Utah, Colorado, and Texas. Using multi-platform observations, we identify the smoke-influenced days with daily maximum 8-h average (MDA8) ozone of 70-85 ppbv in Spokane, Salt Lake City, Denver and Dallas. On these days, mixing of wildfire smoke into urban pollution enhances simulated MDA8 ozone by 10–20 ppbv.

Plain Language Summary (200 words). Wildfires have torn across western North America over the last decade. Smoke from wildland fires in Canada can travel thousands of kilometers to US cities and reacts with urban pollution to create harmful ozone, a criteria pollutant regulated by the US Environmental Protection Agency. Accurately quantifying this impact is needed to inform US air quality policy, but is challenging due to complex physical and chemical processes. In this study, we analyze surface and airborne measurements, alongside a new variable-resolution global chemistry-climate model, to elucidate these processes. We show that conversion of NO_x emissions from wildfires to more oxidized forms reduces their localized impacts on ozone. When Canadian smoke plumes descend towards US cities, including Spokane, Salt Lake City, Denver and Dallas, higher temperatures cause a restoration of NO_x and thus facilitate production of ozone in transit. On days when the observed daily maximum

8-h average ozone exceeds the health-based limit (70 ppbv), mixing of wildfire smoke into urban pollution can contribute 10–20 ppbv.

1. Introduction

Large wildfires have become increasingly common during recent decades in the Canadian province of British Columbia, the US Pacific Northwest, and California, causing severe air pollution, loss of human life, and property damage [*Westerling et al., 2006; Abatzoglou and Williams 2016; Brown et al., 2023*]. Five of the most destructive wildfire seasons of the last half-century occurred in the past seven years: 2017, 2018, 2020, 2021, and 2023, raising the possibility that climate change is already driving changes in fire regimes [*Hagmann et al., 2021; Xie et al., 2020; 2022; Parisien et al., 2023*]. Biomass burning (BB) in wildfires emits particulate matter (PM) along with hundreds of reactive gases, including nitrogen oxides (NO_x), nitrous acid (HONO), carbon monoxide (CO), ammonia (NH_3), and an enormous diversity of volatile organic compounds (VOCs) [*Hatch et al., 2017; Permar et al., 2021; Liang et al., 2022*]. The complex chemical cocktail of wildfire smoke mixed with urban pollution represents a key challenge for understanding fire smoke impacts on secondary air pollutants such as ozone (O_3) [*Jaffe et al., 2020*].

Wildfire emissions have variable impacts on O_3. In a review of more than 100 studies, *Jaffe and Wigder* (2012) found that O_3 is usually enhanced downwind from wildfire plumes with moderate smoke levels, and the O_3 production increases with plume age. At high smoke levels, O_3 formation is suppressed, in part due to low-light conditions or to heterogeneous chemistry on smoke particles [e.g., *Alvarado et al. 2015; Palm et al., 2021*]. Observations show that emissions of HONO and NO_x in boreal and temperate smoke plumes are rapidly (within a few hours after emissions) converted into peroxyacyl nitrates (PANs) and particulate nitrate (pNO_3), such that O_3 production in wildfire plumes rapidly becomes NO_x-limited [*Alvarado et al. 2010; Briggs et al., 2017; Juncosa Calahorrano et al., 2021a; Xu et al., 2021*]. The lifetime of NO_x is approximately one day, while the lifetime of PAN in the mid-troposphere is at least a month [Jacob, 1999]. Once ventilated from a source region to the cold free-troposphere where it is more stable, PAN can be efficiently transported on hemispheric scales [*Lin et al., 2010; Fischer et al., 2014; Fiore et al., 2018*]. When a smoke plume subsides, PAN thermally decomposes to release NO_x and can thus facilitate O_3 formation far downwind [*Liu et al., 2016; Bourgeois et al., 2021*]. Ozone formation is also enhanced when VOC-rich smoke plumes mix into NO_x-rich urban pollution, thereby deteriorating urban air quality [e.g., *McClure & Jaffe 2018; Ninneman & Jaffe 2021; Pan & Fanoola, 2022; Langford et al., 2023*].

Modeling large fire-to-fire variations in emission factors, smoke physics, plume dynamics and complex chemical evolution is challenging [*Paugam et al., 2016; Jaffe et al., 2020; Lindaas et al., 2020; L. Jin et al., 2023; Ye et al., 2021*]. Current chemical transport models (CTMs, with horizontal resolution ranging from 4–200 km) typically overestimate O_3 close to the fires while having difficulty simulating the long-range influence of aged smoke plumes on downwind O_3 [*Singh et al., 2012; Fiore et al., 2014; Zhang et al., 2014; Baker et al., 2016, 2018; Zhang et*

al, 2020; Bourgeois et al., 2021; Tang et al., 2022]. There are large uncertainties in the partitioning of reactive nitrogen (NO_y), with models typically underestimating organic nitrates and PANs in smoke plumes [*Arnold et al., 2015; Cai et al., 2016*]. Recent aircraft field campaigns systematically sampled the first few hours of chemical evolution in wildfire plumes, critical for evaluating and improving models [*Lindaas et al., 2021a*; *Permar et al., 2021*; *Warneke et al., 2023*].

Here we use airborne measurements from the 2018 Western Wildfire Experiment for Cloud Chemistry, Aerosol Absorption, and Nitrogen (WE-CAN) campaign [*Lindaas et al., 2021a*; *Juncosa Calahorrano et al., 2021ab*] to partition BB emissions of NO_y into NO_x, PAN, and NO_3^- (NO_3^- = HNO_3 + *p*NO_3) in a variable-resolution global chemistry-climate model (AM4VR) [*Lin et al., 2024*]. We show that sequestration of NO_x emissions in PAN from wildfires in the Pacific Northwest enhances their downwind impacts on O_3 in US cities designated as O_3 nonattainment areas, including Salt Lake City, Denver and Dallas [US EPA, 2024]. With regional grid refinements providing 13 km resolution over the contiguous US (see Fig.1 in Lin et al., 2024), AM4VR allows us to investigate interactions between urban pollution and smoke plumes from fires thousands of kilometers away in Canada. We assess the contribution of these interactions to the observed high-O_3 episodes by analyzing a suite of model simulations alongside satellite images, aircraft sampling of smoke plumes, and ground-based measurements.

2. Observations and identification of smoke-influenced high-O_3 days

The buildup of O_3 produced from urban emissions under hot and dry meteorological conditions can complicate the attribution of observed O_3 enhancements to smoke influence [*Lin et al., 2017; 2020; Lindaas et al., 2017*]. We identify high-O_3 episodes in Colorado and Texas influenced by Canadian wildfire smoke, using these criteria: (1) Satellite observations show enhancements of Aerosol Optical Depth (AOD) across the Great Plains and animation of the GEOS-R images every 10 minutes shows passage of a cold front towards the Southern Great Plains; via NOAA AerosolWatch (https://star.nesdis.noaa.gov/smcd/spb/aq/AerosolWatch/); (2) Ground sites in Colorado and Texas record $PM_{2.5}$ greater than the 35 μg/m^3 NAAQS level for 24-h mean; (3) IMPROVE ground sites measure enhancements (+50% above background level) in organic aerosol (OA), a key component of wildfire smoke [Garofalo et al., 2019]; and (4) Ground sites measure surface O_3 above the 70 ppbv NAAQS level for daily maximum 8-h average (MDA8).

[Figure 1 about here]

Applying these criteria to data in 2018, we identify smoke-influenced high-O_3 days in the Colorado Front Range Urban Corridor on August 20 and 24, and in the US Deep South on August 20–21 (**Fig.1**). On August 19, GOES-East showed heavy smoke from wildfires burning in the Pacific Northwest (**Fig.1a**). On August 20, a cold front passed across the Great Plains, transporting Canadian wildfire smoke towards the US Deep South (**Fig.1b**). By the afternoon of August 20, smoke had reached Amarillo and Dallas, Texas, and lingered in the region on

the next day, as evidenced from AOD enhancements observed by Suomi-NPP (**Fig.1c-d**). Surface $PM_{2.5}$ levels of 30–60 μg/m^3 for 24-h mean were observed on August 20–21 at sites across the Front Range Urban Corridor, extending from Cheyenne (Wyoming), Fort Collins, Greeley, Longmont, and Denver, Colorado, to Dallas, Texas, while background $PM_{2.5}$ were <10 μg/m^3 at these sites (**Fig.1e-f**). The IMPROVE Rocky Mountain monitor missed the peak smoke on August 20 because measurements are made only every three days. The IMPROVE Wichita Mountains monitor located close to the Oklahoma-Texas border, showed increased OA on August 21, supporting the smoke influence in this region. Surface MDA8 O_3 of 70–85 ppbv were observed at monitors along the smoke transport pathway across Colorado to Texas on August 20–21. During August 22–24, a new cold front transported smoke across the western US, elevating MDA8 O_3, $PM_{2.5}$ and OA in Denver on August 24, but this cold front did not propagate towards the Southern Great Plains. In contrast to the O_3 episodes associated with in-situ production from anthropogenic precursor emissions (e.g. August 1–3), the smoke-influenced high-O_3 episodes exhibit a distinct chemical signature with enhancements in organic-dominated $PM_{2.5}$.

3. GFDL AM4VR simulations

AM4VR is a new variable-resolution global chemistry-climate model recently developed at NOAA's Geophysical Fluid Dynamics Laboratory (GFDL) for research at the nexus of US climate and air quality extremes [*Lin et al., 2024*]. For this study, we conduct nudged AM4VR simulations for 2018 using daily emissions from the Global Fire Emission Database (GFED4s, 0.25ºx0.25º) [*van der Wolf et al., 2017*], distributed vertically between the surface and 6 km based on an injection height climatology derived from MISR (Val Martin et al., 2018). AM4VR includes a revised treatment of VOC emissions [*Lin et al., 2024*], accounting for emissions of acetaldehyde (CH_3CHO) and methyl ethyl ketone (MEK, C_4H_8O), both precursors of PAN, from wildfires that are ignored in our previous model AM4.1 [*Horowitz et al., 2020*]. Anthropogenic emissions are obtained from the Community Emissions Data System version 2021-04-21 (0.1ºx0.1º, O'Rourke et al., 2021).

Four AM4VR model experiments are designed to explore the impacts of oxygenated VOC emissions (OVOC) and NO_y evolution in smoke plumes, in addition to regional anthropogenic emissions (**Table S1**). Fires in our BASE model emit NO_y purely as NO, similar to previous models. *Juncosa Calahorrano* et al. [2021a] showed that, within a few hours after emissions, approximately 37% of the total NO_y species is in the form of PANs and pNO_3 is the second largest contributor (27%), based on data averaged over all fresh plume transects during WE-CAN. Since our model does not fully resolve the rapid chemical transformations within concentrated smoke plumes, we thus parameterize NO_y emissions from fires into 37% PAN, 27% HNO_3, and 36% NO in a second simulation (hereafter AM4VR), as in Lin et al. [2024]. The equilibration between gas-phase HNO_3 and pNO_3 is simulated dynamically depending on temperature, altitude, and NH_3 availability [Fountoukis & Nenes, 2007; Lindass et al., 2021b]. We conduct two additional simulations: one with BB emissions of OVOCs (HCHO, CH_3CHO,

and CH_3COCH_3) increased by a factor of 2 (hereafter OVOCx2), and the other with emissions of NO_y, VOCs, and other gases from fires zeroed out (hereafter noBB). NO_y emissions in the OVOCx2 experiment are treated the same as in BASE.

4. Rapid NO_y evolution slows ozone formation in near-fire smoke plumes

[Figure 2 about here]

We first assess the impacts of NO_y partitioning on O_3 formation in the near-fire (< 1 day of aging) western US smoke plumes sampled by WE-CAN in summer 2018 (Text S1 and Fig.S1). **Fig.2a** shows comparisons of observed and simulated median mixing ratios of PAN between 2.5 and 6 km altitude for each of the WE-CAN flights. The BASE model, with fires emitting NO_y purely as NO, captures only ~50% of the observed PAN abundance. Comparisons of CO, HCHO, CH_3CHO, and CH_3COCH_3 indicate significant under-representation of VOCs in simulated smoke (Text S2 and Fig.S2), consistent with the findings of L. Jin et al. (2023) using the GEOS-Chem model. Doubling OVOC emissions from fires favors PAN formation by producing more acetyl peroxy radical (CH_3CO_3), but it is insufficient to remove the bias, suggesting that CH_3CO_3 has substantial production from oxidation of VOCs not represented by the models (*Coggon et al., 2019; Xu et al., 2021; Permar et al., 2023*). Even at 13 km resolution, it is challenging for the model to capture rapid photochemical processes that occur in a concentrated smoke plume. Using observations to partition a fraction of NO_y emissions from fires into PAN and NO_3^- thus provides a parameterization to account for additional VOCs and rapid chemistry in smoke. The regression slope of simulated PAN with observations increases from 0.51 in BASE to 0.73 in AM4VR with the NO_y partitioning. The overall root-mean-square-error (RMSE) decreases from 160 to 97 pptv.

Fig.2b shows comparison of median O_3 between 2.5 and 6 km altitude in smoke-influenced air masses, identified with observed CO > 85 ppbv, HCN > 275 pptv, and CH_3CN > 200 pptv, for each WE-CAN flight. Rapid conversion of NO_x to PAN and NO_3^- reduces excessive O_3 production in near-fire smoke plumes in the model, decreasing the overall RMSE from 11 to 7 ppbv. The effects are as large as 10–23 ppbv in the fresh smoke plumes sampled on July 26 and August 2, 9 and 13. Supporting our findings, Xu et al. (2021) used a box model constrained by observations to show that the partitioning of NO_y species slows O_3 formation in fresh plumes.

[Figure 3 about here]

We analyze several fresh plumes in more detail. On August 13, the aircraft sampled smoke from wildfires burning in the Salmon Challis National Forest in Idaho (**Fig.S1**). Intercepted at ~4.5 km altitude between 22:00–23:30 UTC, this smoke plume exhibits factors of 2–5 times enhancements of PAN above the background level (**Fig.2c**). On August 2, the aircraft intercepted fresh plumes from fires burning in Southwest Oregon. With the NO_y partitioning, AM4VR captures the observed PAN abundance approaching 3 ppbv on August 13 and 8 ppbv on August 2 within the smoke plumes (**Figs.2c-d**)**.** In contrast, BASE captures less than 30% of observed PAN levels for both plumes. The NO_x loss to NO_3^- and PAN leads to a decrease

of MDA8 O_3 by ~15 ppb in surface air over the burned area around the Idaho/Montana border (**Fig.3a**). The lower O_3 simulated by AM4VR agrees better with WE-CAN observations (**Fig.3d-f**). Doubling OVOC emissions from fires leads to a slight increase in PAN, but this does not systematically reduce model O_3 biases in the fresh plumes. AM4VR also improves upon BASE in representing the observed impacts of aged smoke on MDA8 O_3 exceedances in Salt Lake City on August 13 (**Fig.3a and Fig.S3**).

On July 26, the aircraft sampled smoke from the Carr Fire in the wildland-urban interface of northern California (**Fig.3b-c**). PAN was not measured on this flight. Sampled by multiple aircraft transects at ~4 km altitude between 22:30–24:30 UTC, the smoke plume over northern California exhibited O_3 mixing ratios of 85–120 ppbv, compared to ~65 ppbv in the remote Idaho plume (**Fig.3g**). Fires burning in close proximity to NO_x-rich urban areas in California had a greater impact on O_3 formation. Comparisons of CO and O_3 along the flight track show that AM4VR represents the vertical structure of the smoke plume and the observed magnitude of O_3. The BB NO_y parameterization reduces free tropospheric O_3 by ~23 ppbv in smoke-influenced environments (blue versus red pentagons in **Fig.2b**). This is consistent with box modeling suggesting that O_3 formation in VOC-rich smoke plumes is mostly NO_x-limited [*Xu et al., 2021; X. Jin et al., 2023*].

Evaluation with aircraft observations shows that AM4VR captures the large-scale structure of smoke plumes (e.g., July 26, August 2, and 13). WE-CAN sampled plumes between 2–5 PM (local time) when fires are active and plumes are injected high in the atmosphere. The injection height derived from MISR with a 10:30 AM overpass is thus biased low. However, the simulated vertical distribution of tracers in smoke plumes is not only determined by the MISR injection height climatology but also by strong vertical mixing under hot meteorological conditions. There are cases in which we identified model PAN biases caused by insufficient injection height. On July 30 (stars in Fig.2a-b), for example, the aircraft intercepted fresh smoke plumes at 3–4 km altitude between 22:00–25:00 UTC, while the model simulated plumes at ~2 km altitude (**Fig.S4**). Despite this bias in altitude, the NO_y partitioning consistently leads to enhanced PAN and reduced O_3 in the simulated fresh plumes.

5. Ozone formation in aged smoke plumes in cities

[Figure 4 about here]

We next examine the influence of smoke plumes on O_3 photochemistry in urban areas, following long-range transport over thousands of kilometers. We focus on the August 16–24 period when several cold fronts transported smoke from numerous fires burning in the Pacific Northwest to Salt Lake City, the Colorado Front Range Urban Corridor, and the US Deep South (**Fig.4**). Air quality monitors in Washington state recorded hazardous $PM_{2.5}$ pollution of 100–250 μg/m^3 for 24-h average on August 19–20. Dense wildfire smoke reduced the intensity of light reaching the surface (**Fig.1**) and increased removal of HO_x radicals on smoke particles, leading to observed suppression of O_3 formation in the region on August 20 (**Fig.5**). AM4VR

accounts for the radiative effects of simulated aerosols on photolysis rates and heterogeneous chemistry on smoke particles [*Lin et al.*, 2024]. But AM4VR with GFED4s emissions captures only 60% of the peak $PM_{2.5}$ levels in Washington state, which partly explains model overestimation of O_3 there on August 20. Enhancements of O_3 in aged wildfire smoke are often greatest when smoke levels are moderate (*Buysse et al., 2019; Pan and Faloona, 2022*). On August 16 and 22, when $PM_{2.5}$ was 30–60 μg/m^3, both observations and model showed elevated MDA8 O_3 above 70 ppbv at monitors in Spokane, Richland-Kennewick, and Portland.

[Figure 5 about here]

Comparisons of surface MDA8 O_3 from the noBB, BASE, and AM4VR experiments demonstrate the critical role of NO_x supply from PAN decomposition and urban pollution on O_3 formation in VOC-rich smoke plumes (**Fig.5**). On August 16 (**Fig.5a**), observed MDA8 O_3 is 80 ppbv at Spokane and 85 ppbv at Richland-Kennewick. Simulated MDA8 O_3 is below 60 ppbv in the noBB experiment, indicating minor influence of O_3 produced from local anthropogenic emissions alone. Accounting for VOC and NO_x emissions from fires, simulated MDA8 O_3 increases to 70–75 ppbv in BASE, still lower than observed. Accounting for enhanced PAN formation in fresh plumes and its subsequent decomposition to NO_x in aged smoke increases MDA8 O_3 by ~5 ppbv in AM4VR, bringing it closer to the observed values. Similarly, the NO_y partitioning led to better agreements of simulated MDA8 O_3 with observations at Richland-Kennewick, Portland, and Mt. Bachelor Observatory on August 22. MDA8 O_3 is 70–80 ppbv from observations, below 55 ppbv in noBB, 55–65 ppbv in BASE, and 70–75 ppbv in AM4VR (**Fig.5b**).

On August 20–21, as smoke descended in the dry air stream of the cold front towards higher temperatures in the US Deep South (**Fig.1 and Fig.4d**), PAN decomposed to release NO_x and thus facilitated O_3 formation (**Fig.5c**). This is clearly demonstrated with the substantial difference between the O_3 simulated in BASE versus AM4VR. The BASE model simulates MDA8 O_3 below 70 ppbv in Denver, Amarillo, and Dallas, inconsistent with observations. With NO_y parameterization, AM4VR simulates well the observed O_3 levels in these areas, increasing MDA8 O_3 by ~8 ppbv relative to BASE and 10–15 ppbv relative to noBB. Most of the sites with observed MDA8 O_3 exceeding 70 ppbv were located downwind of the Denver and Dallas urban areas along the smoke transport pathway, indicating in-situ O_3 production resulting from mixing of smoke VOCs with urban NO_x. During August 21, as smoke further mixed into surface air in Dallas (**Fig.1d**), urban pollution provided a critical NO_x supply to enhance O_3 formation in smoke by ~5 ppbv (**Fig.S5**).

[Fig.6 about here]

During August 23–24, a new cold front transported smoke towards Salt Lake City, Denver, and California's Central Valley (**Fig.4f** and **Fig.6**). Smoke plumes were intercepted by the WE-CAN aircraft below ~4 km during the ascent from Boise at 2:00PM PDT (21:00 UTC), between 1–3 km off the California coast at 3–6 PM PDT, and below ~4 km during the descent to Boise at 7:30PM (**Figs.6a-b**). The estimated chemical age is 1–3 days for the plumes over Boise and >

3 days for the plume off the California coast [O'Dell et al., 2020; Permar et al., 2023]. These aged smoke plumes exhibit relatively lower PAN and higher O_3 levels compared to the fresh plumes sampled by WE-CAN (**Fig.2**). The plume off the California coast exhibits O_3 above 100 ppbv and PAN below 0.5 ppbv. AM4VR with NO_y parameterization captures better enhancements of O_3 with increased plume age, simulating higher O_3 in aged smoke off the California coast than BASE (**Fig.6b vs 6d**).

As the smoke plumes wafted across the western US and mixed with urban pollution, observations show MDA8 O_3 increased by 10–20 ppbv in Salt Lake City on August 23 and in the Colorado Front Range on August 24 relative to August 22 (**Fig.6e**). AM4VR captures the observed features, simulating increased O_3 in the descending dry air stream of the cold front. With BB emissions of VOCs and NO_y zeroed out, simulated O_3 decreased in Salt Lake City on August 23 and in Colorado on August 24, indicating that the cold front would otherwise transport clean air to these areas in the absence of wildfire smoke (**Fig.6f**). Over Oklahoma and northern Texas, in contrast, noBB showed enhanced MDA8 O_3 on August 23-24, indicating that the ozone pollution was primarily produced from regional anthropogenic emissions. The model attribution is consistent with IMPROVE observations showing little OA enhancement at Wichita Mountain on August 24 (**Fig.1f**). California's Central Coast and San Joaquin Valley were also influenced by smoke ($PM_{2.5}$ = 35–50 μg/m^3) on August 24 **(Fig.S6).** Observations show increased sites in California with MDA8 O_3 exceeding 70 ppbv on the smoky day. AM4VR simulates 3–6 ppbv MDA8 O_3 enhancements due to wildfire emissions, implying that the exceedances would not occur if there were no smoke.

6. Conclusions

Due to the large quantity of VOCs emitted by wildfires, O_3 formation in aged smoke is generally NO_x-limited. Through an integrated analysis of observations and global model simulations, we highlight the role of NO_y evolution on O_3 production in aged smoke plumes transported thousands of kilometers downwind. Rapid conversion of NO_x to NO_3^- and PAN reduces excessive O_3 production in the model in near-fire smoke plumes sampled by the WE-CAN aircraft campaign. Sequestration of NO_x to PAN from boreal fires fuels downwind O_3 formation. When smoke plumes travel from British Columbia to US cities, including Spokane, Portland, Salt Lake City, Denver, and Dallas, PAN thermally decomposes to release NO_x and thus enhances O_3 production in conjunction with the urban NO_x supply. On days when observed MDA8 O_3 is 70–85 ppbv, mixing of wildfire smoke into urban pollution enhances O_3 production by 10–20 ppbv. As large wildfires are projected to increase in western North America due to climate warming [Xie et al., 2022], accurate representation of VOCs and NO_y evolution in smoke is critical to assess the implications for US O_3 air quality.

Open Research.

Source code of GFDL AM4VR is available at https://zenodo.org/records/10257866. WE-CAN data is available at https://data.eol.ucar.edu/master_lists/generated/we-can/. Surface observations of $PM_{2.5}$ and O_3 are available at https://aqs.epa.gov/aqsweb/airdata/download_files.html.

Acknowledgements: We thank Songmiao Fan, Emily Fischer, Frank Flocke, Daniel A. Jaffe and Rui Wang for helpful comments. Funding for the WE-CAN data collection was provided by the US National Science Foundation (NSF award numbers: AGS-1650786, AGS-1650275, AGS-1950327, and AGS-1652688) and the US National Oceanic and Atmospheric Administration (NOAA) under award numbers NA17OAR4310010 and NA17OAR4310001. L.H. and W.P. were also supported by NSF grants AGS-2144896 and EPSCoR-2242802.

References:

Alvarado, M. J., J. A. Logan, J. Mao, et al. 2010. Nitrogen oxides and PAN in plumes from boreal fires during ARCTAS-B and their impact on ozone: an integrated analysis of aircraft and satellite observations. Atmos. Chem. Phys. 10 (20):9739-9760. doi: 10.5194/acp-10-9739-2010.

Alvarado, M. J., C. R. Lonsdale, R. J. Yokelson, et al., 2015. Investigating the links between ozone and organic aerosol chemistry in a biomass burning plume from a prescribed fire in California chaparral. Atmos. Chem. Phys. 15 (12):6667-6688. doi: 10.5194/acp-15-6667-2015.

Arnold, S. R., Emmons, L. K., Monks, S. A., et al: Biomass burning influence on high-latitude tropospheric ozone and reactive nitrogen in summer 2008: a multi-model analysis based on POLMIP simulations, Atmos. Chem. Phys., 15, 6047–6068, https://doi.org/10.5194/acp-15-6047-2015, 2015.

Abatzoglou, J. T. and Williams, A. P.: Impact of anthropogenic climate change on wildfire across western US forests, P. Natl. Acad. Sci. USA, 113, 11770–11775, doi:10.1073/pnas.1607171113, 2016.

Baker, K. R., Woody, M. C., Tonnesen, G. S. et al.: Contribution of regional-scale fire events to ozone and PM2.5 air quality estimated by photochemical modeling approaches, Atmos. Environ.,140, 539–554, doi:10.1016/j.atmosenv.2016.06.032, 2016

Baker, K. R., Woody, M. C., Valin, L. et al.: Photochemical model evaluation of 2013 California wildfire air quality impacts using surface, aircraft, and satellite data, Sci. Total Environ., 637, 1137–1149, https://doi.org/10.1016/j.scitotenv.2018.05.048, 2018.

Bourgeois I. et al., Large contribution of biomass burning emissions to ozone throughout the global remote troposphere. Proc. Natl. Acad. Sci. U.S.A. 118, e2109628118 (2021).

Briggs, N. L., D. A. Jaffe, H. L. Gao, J. R. Hee, P. M. Baylon, Q. Zhang, S. Zhou, S. C. Collier, P. D. Sampson, and R. A. Cary. 2016. Particulate matter, ozone, and nitrogen species in aged wildfire plumes observed at the Mount Bachelor Observatory. Aerosol Air Qual. Res. 16 (12), 3075-3087. doi: 10.4209/aaqr.2016.03.0120.

Brown, P.T., Hanley, H., Mahesh, A. *et al.* Climate warming increases extreme daily wildfire growth risk in California. *Nature* 621, 760–766 (2023). https://doi.org/10.1038/s41586-023-06444-3

Buysse, C. E., A. Kaulfus, U. Nair, and D. A. Jaffe. 2019. Relationships between particulate matter, ozone, and nitrogen oxides during urban smoke events in the western US. Environ. Sci. Technol. doi: 10.1021/acs.est.9b05241.

Cai, C. X., S. Kulkarni, Z. Zhao, A. P. Kaduwela, J. C. Avise et al. (2016). Simulating reactive nitrogen, carbon monoxide, and ozone in California during ARCTAS-CARB 2008 with high wildfire activity. Atmos. Environ. 128:28-44. doi: 10.1016/j.atmosenv.2015.12.031.

Coggon, M. M., C. Y. Lim, A. R. Koss, K. Sekimoto et al. (2019): OH chemistry of non-methane organic gases (NMOGs) emitted from laboratory and ambient biomass burning smoke: evaluating the influence of furans and oxygenated aromatics on ozone and secondary NMOG formation. Atmos. Chem. Phys. 19 (23):14875-14899. doi: 10.5194/acp-19-14875-2019.

Fiore, AM, J.T. Oberman, M.Y. Lin et al. (2014): Estimating North American background ozone in U.S. surface air with two independent global models: Variability, uncertainties, and recommendations, Atmos. Environ., 96, 284-300, doi: 10.1016/j.atmosenv.2014.07.045

Fiore, A.M., E.V. Fischer, G.P. Milly, et al. 2018.: Peroxy acetyl nitrate (PAN) measurements at northern midlatitude mountain sites in April: a constraint on continental source-receptor relationships. Atmos. Chem. Phys., 18, no. 20, 15345-15361, doi:10.5194/acp-18-15345-2018.

Fischer, E. V.; Jacob, D. J.; Yantosca, R. M. et al.: Atmospheric Peroxyacetyl Nitrate (PAN): A Global Budget and Source Attribution. Atmospheric Chemistry and Physics 2014, 14 (5), 2679– 2698, DOI: 10.5194/acp-14-2679-2014

Fountoukis, C. and Nenes, A.: ISORROPIA II: a computationally efficient thermodynamic equilibrium model for K^+–Ca^{2+}–Mg^{2+}–NH^{4+}–Na^+–SO_4^{2-}–NO^{3-}–Cl^-–H_2O aerosols, Atmos. Chem. Phys., 7, 4639–4659, https://doi.org/10.5194/acp-7-4639-2007, 2007.

Garofalo, L. A., Matson A. Pothier, Ezra J. T. Levin, Teresa Campos, Sonia M. Kreidenweis, and Delphine K. Farmer. Emission and Evolution of Submicron Organic Aerosol in Smoke from Wildfires in the Western United States, ACS Earth and Space Chemistry 2019, 3 (7), 1237-1247, DOI: 10.1021/acsearthspacechem.9b00125

Hatch, L. E., R. J. Yokelson, C. E. Stockwell, P. R. Veres, I. J. Simpson, D. R. Blake, J. J. Orlando, and K. C. Barsanti. 2017. Multi-instrument comparison and compilation of non-methane organic gas emissions from biomass burning and implications for smoke-derived secondary organic aerosol precursors. Atmos. Chem. Phys. 17 (2):1471-1489. doi: 10.5194/acp-17-1471-2017.

Hagmann, R. K. et al. Evidence for widespread changes in the structure, composition, and fire regimes of western North American forests. Ecol. Appl. 31, e02431. https://doi.org/10.1002/eap.2431 (2021).

Horowitz, L.W. et al. (2020): The GFDL Global Atmospheric Chemistry-Climate Model AM4.1: Model Description and Simulation Characteristics. Journal of Advances in Modeling Earth Systems, 12(10), DOI:10.1029/2019MS002032.

Jacob D. (1999); *Introduction to Atmospheric Chemistry*. Page 212-215. Princeton University Press.

Jaffe, D. A., and N. L. Wigder. 2012. Ozone production from wildfires: A critical review. Atmos. Environ. 51:1-10. doi: 10.1016/j.atmosenv.2011.11.063.

Jaffe, Daniel A., Susan M. O'Neill, Narasimhan K. Larkin, Amara L. Holder, David L. Peterson, Jessica E. Halofsky & Ana G. Rappold (2020). Wildfire and prescribed burning impacts on air quality in the United States, Journal of the Air & Waste Management Association, 70:6, 583-615, DOI: 10.1080/10962247.2020.1749731

Juncosa Calahorrano, J. F., Lindaas, J., O'Dell, K., Palm, B. B., Peng, Q., Flocke, F., et al. (2021a). Daytime oxidized reactive nitrogen partitioning in western U.S. wildfire smoke plumes. Journal of Geophysical Research: Atmospheres, 126, e2020JD033484. https://doi.org/10.1029/2020JD033484

Juncosa Calahorrano, J., V. H. Payne, S. S. Kulawik, B. Ford, F. M. Flocke, T. Campos, and E. V. Fischer (2021b), Evolution of Peroxyacetyl Nitrate (PAN) in wildfire smoke plumes detected by the Cross-Track Infrared Sounder (CrIS) over the western U.S. during summer 2018, Geophysical Research Letters, https://agupubs.onlinelibrary.wiley.com/doi/10.1029/2021GL093405.

Jin, L., Permar, W., Selimovic, V. et al: Constraining emissions of volatile organic compounds from western US wildfires with WE-CAN and FIREX-AQ airborne observations, Atmos. Chem. Phys., 23, 5969–5991, https://doi.org/10.5194/acp-23-5969-2023, 2023.

433 Jin, X., A. M. Fiore, and R. C. Cohen. Space-Based Observations of Ozone Precursors within
434 California Wildfire Plumes and the Impacts on Ozone-NOx-VOC Chemistry Environmental
435 Science & Technology, 57 (39), 14648-14660, DOI: 10.1021/acs.est.3c04411, 2023
436 Langford, A. O., Senff, C. J., Alvarez, R. J. II, Aikin, K. C., Ahmadov, R., Angevine, W. M., et al.
437 (2023). Were wildfires responsible for the unusually high surface ozone in Colorado during
438 2021? Journal of Geophysical Research: Atmospheres, 128, e2022JD037700.
439 https://doi.org/10.1029/2022JD037700
440 Liang, Y., Stamatis, C., Fortner, E. C., Wernis, R. A. et al: Emissions of organic compounds from
441 western US wildfires and their near-fire transformations, Atmos. Chem. Phys., 22, 9877–9893,
442 https://doi.org/10.5194/acp-22-9877-2022, 2022.
443 Lin, M., T. Holloway, G. R. Carmichael and A. M. Fiore: Quantifying pollution inflow and outflow over
444 East Asia in spring with regional and global models. Atmos. Chem. Phys., 10, 4221-4239,
445 2010.
446 Lin, M. et al. (2017), US surface ozone trends and extremes over 1980-2014: Quantifying the roles of
447 rising Asian emissions, domestic controls, wildfires, and climate. Atmos. Chem. Phys., 17 (4),
448 doi:10.5194/acp-17-2943-2017.
449 Lin, M., et al. (2020): Vegetation feedbacks during drought exacerbate ozone air pollution extremes in
450 Europe. Nature Climate Change, 10(5), DOI:10.1038/s41558-020-0743-y.
451 Lin, M., L. W. Horowitz, M. Zhao, L. Harris, P. Ginoux, J. P. Dunne, S. Malyshev, E. Shevliakova, H.
452 Ahsan, S. Garner, F. Paulot, A. Pouyaei, S. J. Smith, Y. Xie, N. Zadeh, L. Zhou. The GFDL
453 Variable-Resolution Global Chemistry-Climate Model for Research at the Nexus of US Climate
454 and Air Quality Extremes. Journal of Advances in Modeling Earth Systems, in press,
455 https://doi.org/10.1029/2023MS003984, 2024. Full text available here.
456 Lindaas, J., D. K. Farmer, I. B. Pollack et al. (2017), The impact of aged wildfire smoke on atmospheric
457 composition and ozone in the Colorado Front Range in summer 2015, Atmos. Chem. Phys.,
458 https://doi.org/10.5194/acp-2017-171.
459 Lindaas, J.; Pollack, I. B.; Garofalo, L. A. et al (2021a): Emissions of Reactive Nitrogen From Western
460 U.S. Wildfires During Summer 2018. J. Geophys Res. Atmospheres, 2021, 126 (2). DOI:
461 10.1029/2020JD032657
462 Lindaas, J., Pollack, I. B., Calahorrano, J. J., O'Dell, K., Garofalo, L. A., Pothier, M. A., et al. (2021b).
463 Empirical insights into the fate of ammonia in western U.S. wildfire smoke plumes. Journal of
464 Geophysical Research: Atmospheres, 126, e2020JD033730.
465 https://doi.org/10.1029/2020JD033730
466 Liu, X., et al. (2016), Agricultural fires in the southeastern US during SEAC(4)RS: Emissions of trace
467 gases and particles and evolution of ozone, reactive nitrogen, and organic aerosol, J.
468 Geophys. Res.-Atmos., 121(12), 7383-7414, doi:10.1002/2016jd025040
469 McClure and Jaffe (2018): Investigation of high ozone events due to wildfire smoke in an urban area,
470 Atmospheric Environment 194 (2018), 146–157, doi:10.1016/j.atmosenv.2018.09.021
471 Ninneman, M.; Jaffe, D. A. The Impact of Wildfire Smoke on Ozone Production in an Urban Area:
472 Insights from Field Observations and Photochemical Box Modeling. Atmos. Environ. 2021,
473 267, 118764 DOI: 10.1016/j.atmosenv.2021.118764
474 O'Dell, K., R. Hornbrook, W. Permar et al. (2020), Hazardous air pollutants in fresh and aged western
475 U.S. wildfire smoke and implications for long-term exposure, Environmental Science &
476 Technology, https://doi.org/10.1021/acs.est.0c04497.
477 O'Rourke, P. R, Smith, S. J., Mott, A., Ahsan, H., McDuffie, E. E., Crippa, M., Klimont, S., McDonald,
478 B., Z., Wang, Nicholson, M. B, Feng, L., and Hoesly, R. M. (2021, April 21). CEDS v-2021-04-

21 Emission Data 1975-2019 (Version 04-21-2021). https://data.pnnl.gov/dataset/CEDS-4-21-21.

Pan, K. and Faloona, I. C.: The impacts of wildfires on ozone production and boundary layer dynamics in California's Central Valley, Atmos. Chem. Phys., 22, 9681–9702, https://doi.org/10.5194/acp-22-9681-2022, 2022.

Parisien, MA., Barber, Q.E., Bourbonnais, M.L. et al. Abrupt, climate-induced increase in wildfires in British Columbia since the mid-2000s. Commun Earth Environ 4, 309 (2023). https://doi.org/10.1038/s43247-023-00977-1

Paugam, R., M. Wooster, S. Freitas, and M. V. Martin (2016), A review of approaches to estimate wildfire plume injection height within large-scale atmospheric chemical transport models, Atmos. Chem. Phys., 16(2), 907-925, doi:10.5194/acp-16-907-2016

Palm, B. B., Peng, Q., Hall, S. R., Ullmann, K., Campos, T. L., Weinheimer, A., et al. (2021). Spatially resolved photochemistry impacts emissions estimates in fresh wildfire plumes. Geophysical Research Letters, 48, e2021GL095443. https://doi.org/10.1029/2021GL095443

Permar, W., Q. Wang, V. Selimovic, C. Wielgasz, R. J. Yokelson, R. S. Hornbrook, A. J. Hills, E. C. Apel, I.-T. Ku, Y. Zhou, B. C. Sive, A. P. Sullivan, J. L. Collett Jr., T. L. Campos, B. B. Palm, Q. Peng, J. A. Thornton, L. A. Garofalo, D. K. Farmer, S. M. Kreidenweis, E. J. T. Levin, P. J. DeMott, F. Flocke, E. V. Fischer, and L. Hu (2021), Emissions of trace organic gases from western U.S. wildfires based on WE-CAN aircraft measurements,126, e2020JD033838. https://doi.org/10.1029/2020JD033838

Permar, W., Jin, L., Peng, Q., O'Dell, K., Lill, E., Selimovic, V., Yokelson, R. J., Hornbrook, R. S., Hills, A. J., Apel, E. C., Ku, I.-T., Zhou, Y., Sive, B. C., Sullivan, A. P., Collett, J. L., Palm, B. B., Thornton, J. A., Flocke, F., Fischer, E. V., and Hu, L.: Atmospheric OH reactivity in the western United States determined from comprehensive gas-phase measurements during WE-CAN, Environ. Sci. Atmos., 3, 97–114, https://doi.org/10.1039/D2EA00063F, 2023.

Singh, H. B., C. Cai, A. Kaduwela, A. Weinheimer, and A. Wisthaler (2012), Interactions of fire emissions and urban pollution over California: Ozone formations and air quality simulations, Atmos Environ., 56, 45-51, doi:10/1016/j.atmosenv.2012.03.046.

Tang, W., Emmons, L. K., Buchholz, R. R., Wiedinmyer, C., Schwantes, R. H., He, C., … Campos, T. L. (2022). Effects of fire diurnal variation and plume rise on U.S. air quality during FIREX-AQ and WE-CAN based on the Multi-Scale Infrastructure for Chemistry and Aerosols (MUSICAv0). Journal Of Geophysical Research: Atmospheres, 127, e2022JD036650. doi:10.1029/2022JD036650

US EPA 2024. 8-Hour Ozone Nonattainment Areas for the 2015 National Ambient Air Quality Standards (NAAQS). https://www3.epa.gov/airquality/greenbook/map8hr_2015.html

Val Martin, M., Kahn, R., & Tosca, M. (2018). A global analysis of wildfire smoke injection heights derived from space-based multi-angle imaging. Remote Sensing, 10(10), 1609. https://doi.org/10.3390/rs10101609

van der Werf, G. R., Randerson, J. T., Giglio, L. et al. (2017). Global fire emissions estimates during 1997–2016. Earth System Science Data, 9(2), 697–720. https://doi.org/10.5194/essd-9-697-2017. Latest data for 1997-2023 available at https://www.geo.vu.nl/~gwerf/GFED/GFED4/, last assessed October 1, 2022.

Warneke, C., Schwarz, J. P., Dibb, J., Kalashnikova, O., Frost, G., Al-Saad, J., et al. (2023). Fire influence on regional to global environments and air quality (FIREX-AQ). Journal of Geophysical Research: Atmospheres, 128, e2022JD037758. https://doi.org/10.1029/2022JD037758

Westerling, A. L.; Hidalgo, H. G.; Cayan, D. R.; Swetnam, T. W. Warming and Earlier Spring Increase Western US Forest Wildfire Activity. Science 2006, 313 (5789), 940– 943, DOI: 10.1126/science.1128834

Xie, Y., M. Lin, and L.W. Horowitz (2020): Summer $PM_{2.5}$ Pollution Extremes Caused by Wildfires Over the Western United States During 2017–2018. Geophys. Res. Lett., 47(16), DOI:10.1029/2020GL089429.

Xie, Y., M. Lin, Bertrand Decharme, Christine Delire, Larry W. Horowitz, David M. Lawrence, Fang Li, Roland Séférian (2021). Tripling of western US particulate pollution from wildfires in a warming climate. Proc. Natl Acad. Sci. USA 119, e2111372119 (2022).

Xu, L., J.D. Crounse, K.T. Vasquez, et al. Ozone Chemistry in Western U.S. Wildfire Plumes. Science Advances, 7(50), https://doi.org/10.1126/sciadv.abl3648, 2021.

Ye, X., Arab, P., Ahmadov, R., et al.: Evaluation and intercomparison of wildfire smoke forecasts from multiple modeling systems for the 2019 Williams Flats fire, Atmos. Chem. Phys., 21, 14427–14469, https://doi.org/10.5194/acp-21-14427-2021, 2021.

Zhang, L., Jacob, D. J., Yue, X., Downey, N. V., Wood, D. A., and Blewitt, D.: Sources contributing to background surface ozone in the US Intermountain West, Atmos. Chem. Phys., 14, 5295–5309, doi:10.5194/acp-14-5295-2014, 2014

Zhang, L., Lin, M., Langford, A. O., Horowitz, L. W., Senff, C. J., Klovenski, E., Wang, Y., Alvarez II, R. J., Petropavlovskikh, I., Cullis, P., Sterling, C. W., Peischl, J., Ryerson, T. B., Brown, S. S., Decker, Z. C. J., Kirgis, G., and Conley, S.: Characterizing sources of high surface ozone events in the southwestern US with intensive field measurements and two global models, Atmos. Chem. Phys., 20, 10379–10400, https://doi.org/10.5194/acp-20-10379-2020, 2020

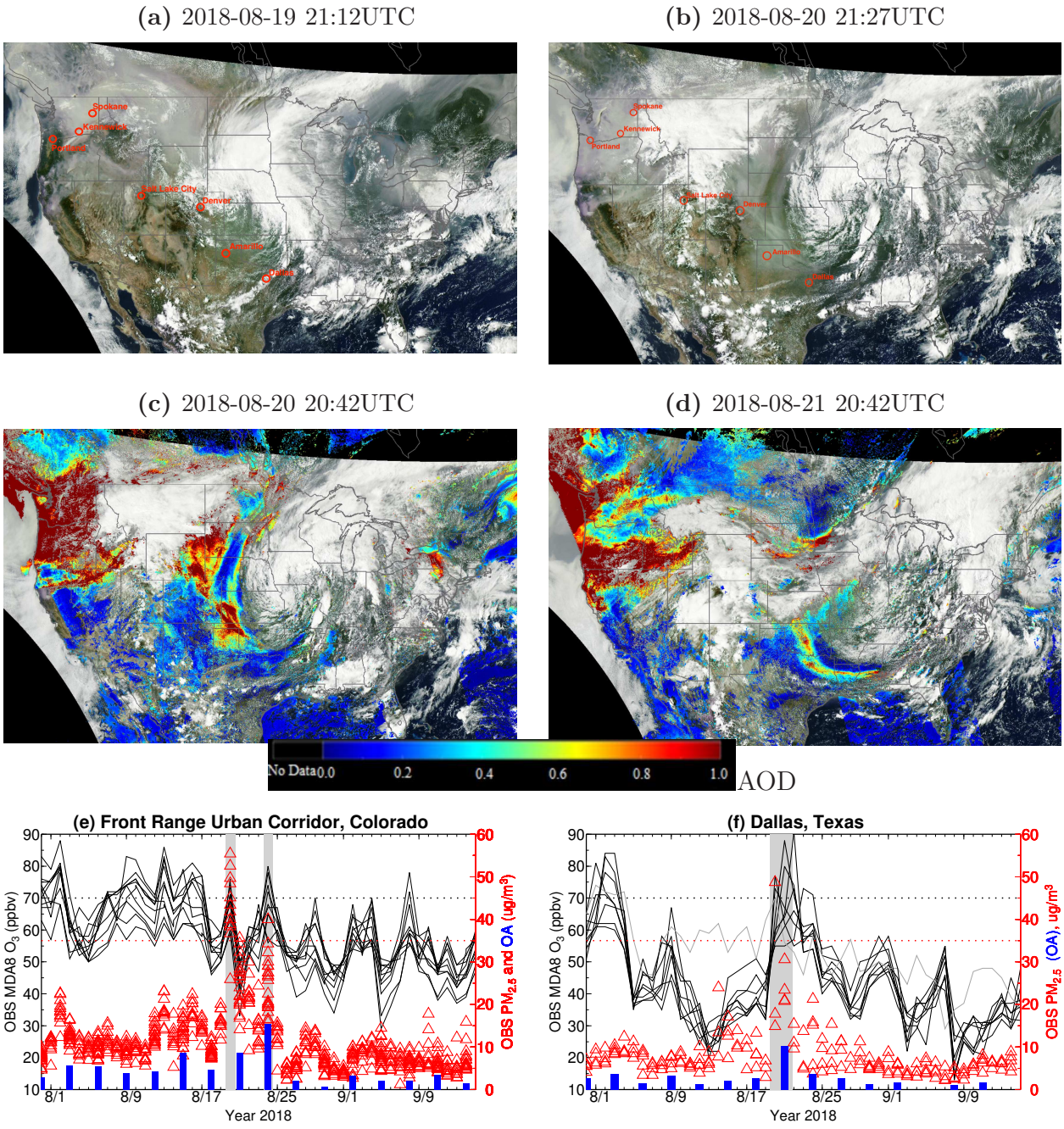

Figure 1. (a-b) GOES images on August 19 and 20, 2018. Cities referenced in the article are labeled. (c-d) Suomi-NPP AOD superimposed on the GOES images on August 20 and 21, 2018. (e-f) Time series of observed daily MDA8 O_3 (black lines) and 24-h $PM_{2.5}$ (red triangles) at AQS sites in the Front Range Urban Corridor, Colorado and Dallas, Texas. Also shown is O_3 at Amarillo, Texas (gray line). Blue bars show organic aerosols measured by IMPROVE at Rocky Mountain, Colorado and Wichita Mountains, Oklahoma.

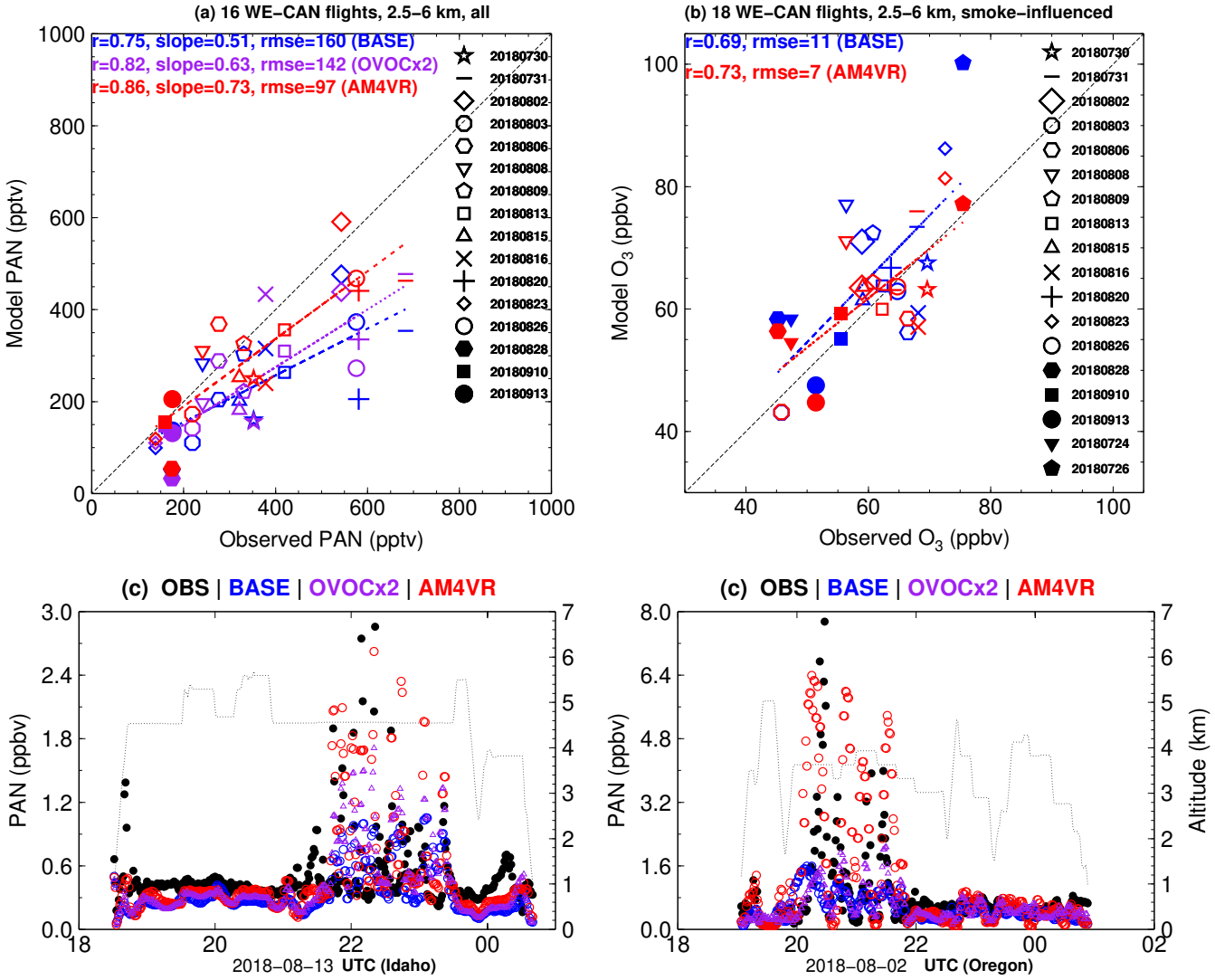

Figure 2. (a) Scatter plots of observed and simulated median mixing ratios of PAN during WE-CAN: each dot represents average of all data between 2.5-6 km altitude for each flight. Results are shown for BASE with BB emitting NO_y as 100% NO (blue), for doubling OVOC BB emissions (purple), and for AM4VR (red) with BB emitting NO (36%), HNO_3 (27%), and PAN (37%); (b) Same as (a) but for median O_3 in smoke-influenced observations (see text) for each WE-CAN flight; (c,d) Comparison of observed and simulated PAN along the WE-CAN flights on August 13 and 2. Dotted lines denote flight altitude using right axis.

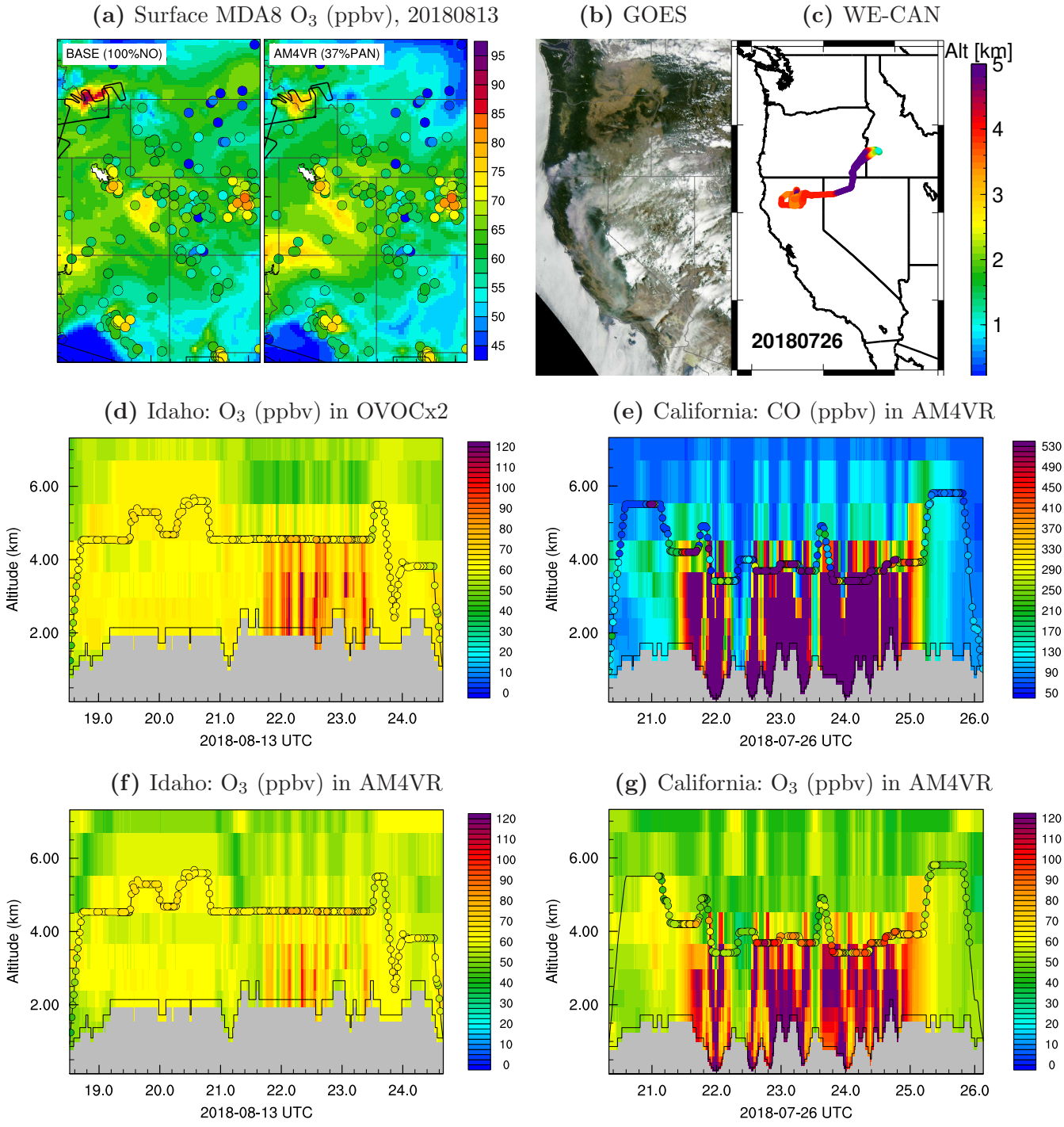

Figure 3. (a) Maps of surface MDA8 O_3 on August 13 from BASE (left) and AM4VR (right) simulations, with color-coded circles representing AQS observations. Thick black lines denote the flight track. (b,c) GOES image and WE-CAN flight on July 26. (d,f) Ozone observed on the August 13 flight superimposed on the time-height curtain plot of O_3 from the OVOCx2 and AM4VR experiments. (e,g) Observed and AM4VR simulated CO and O_3 for the July 26 flight.

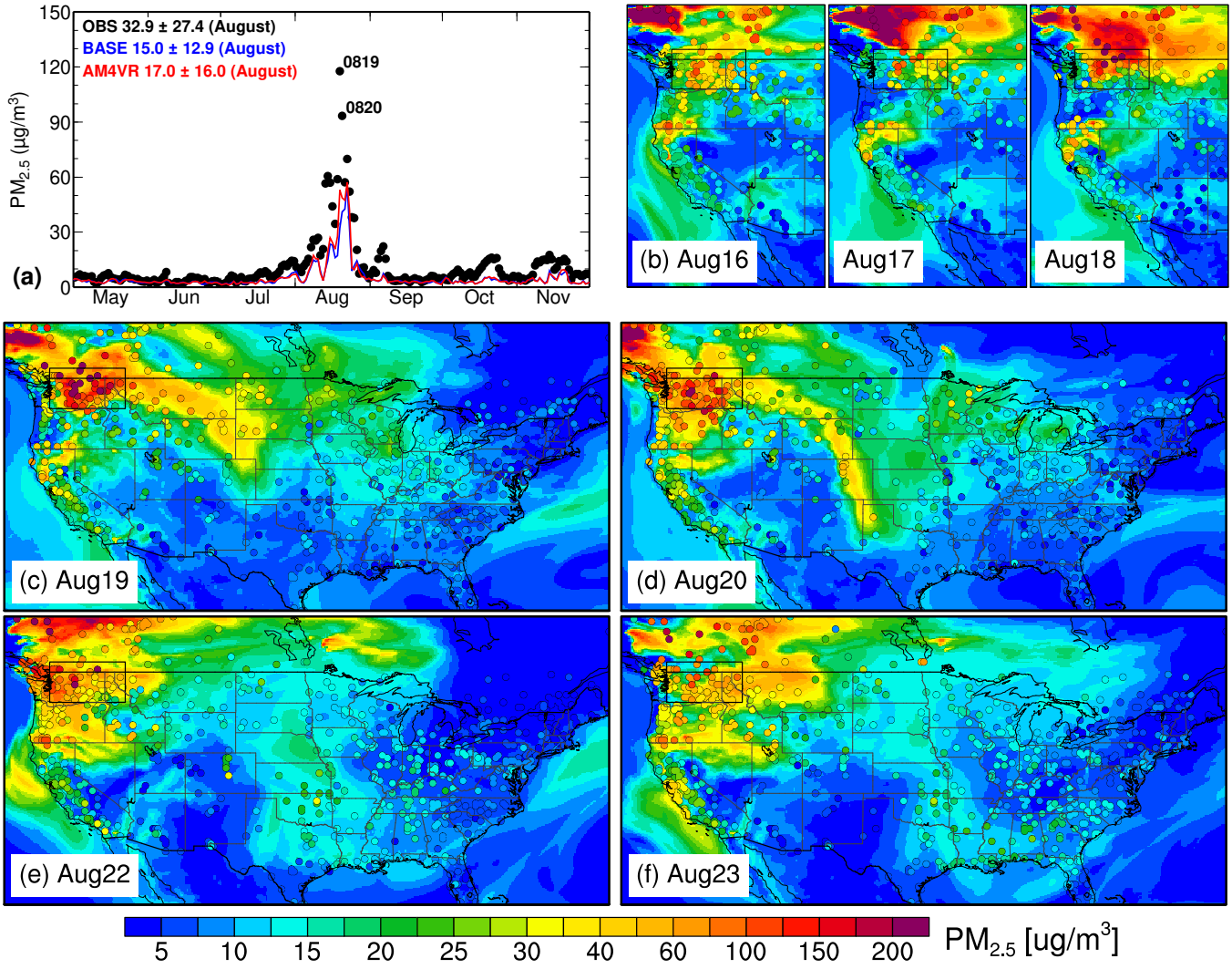

Figure 4. (a) Time series of 24-h mean surface $PM_{2.5}$ averaged over AQS sites in Washington state (box on map). (b-f) Maps of 24-h mean $PM_{2.5}$ from observations (filled circles) and AM4VR simulations (shading) on August 16-18 over the western US, and August 19-23 over the contiguous US.

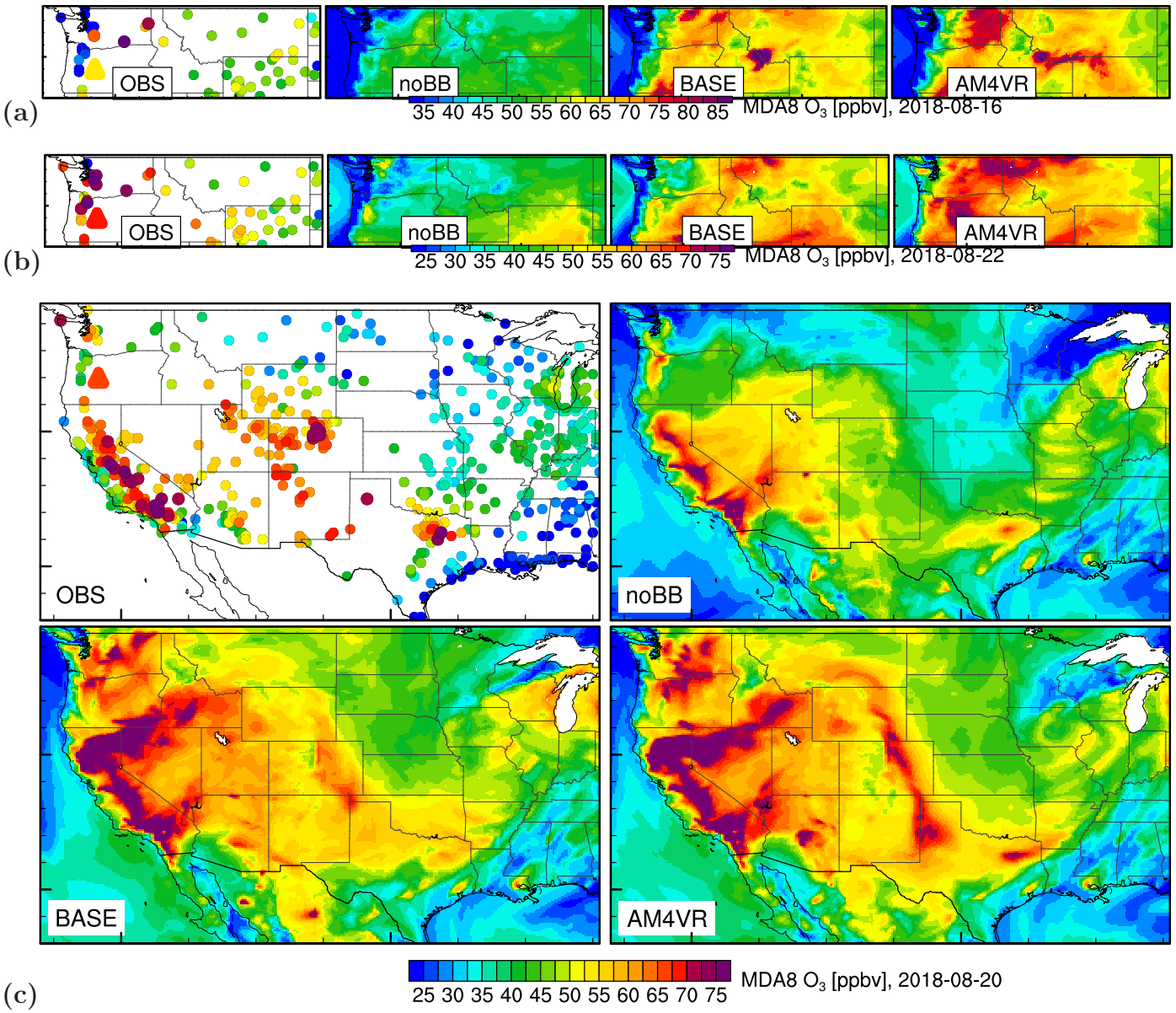

Figure 5. Surface MDA8 O_3 concentrations on August 16, 22 and 20 of 2018 from observations and model simulations with BB emissions of all NO_y and VOCs zero out (noBB), with BB emitting NO_y as 100% NO (BASE), and with AM4VR including the NO_y partitioning.

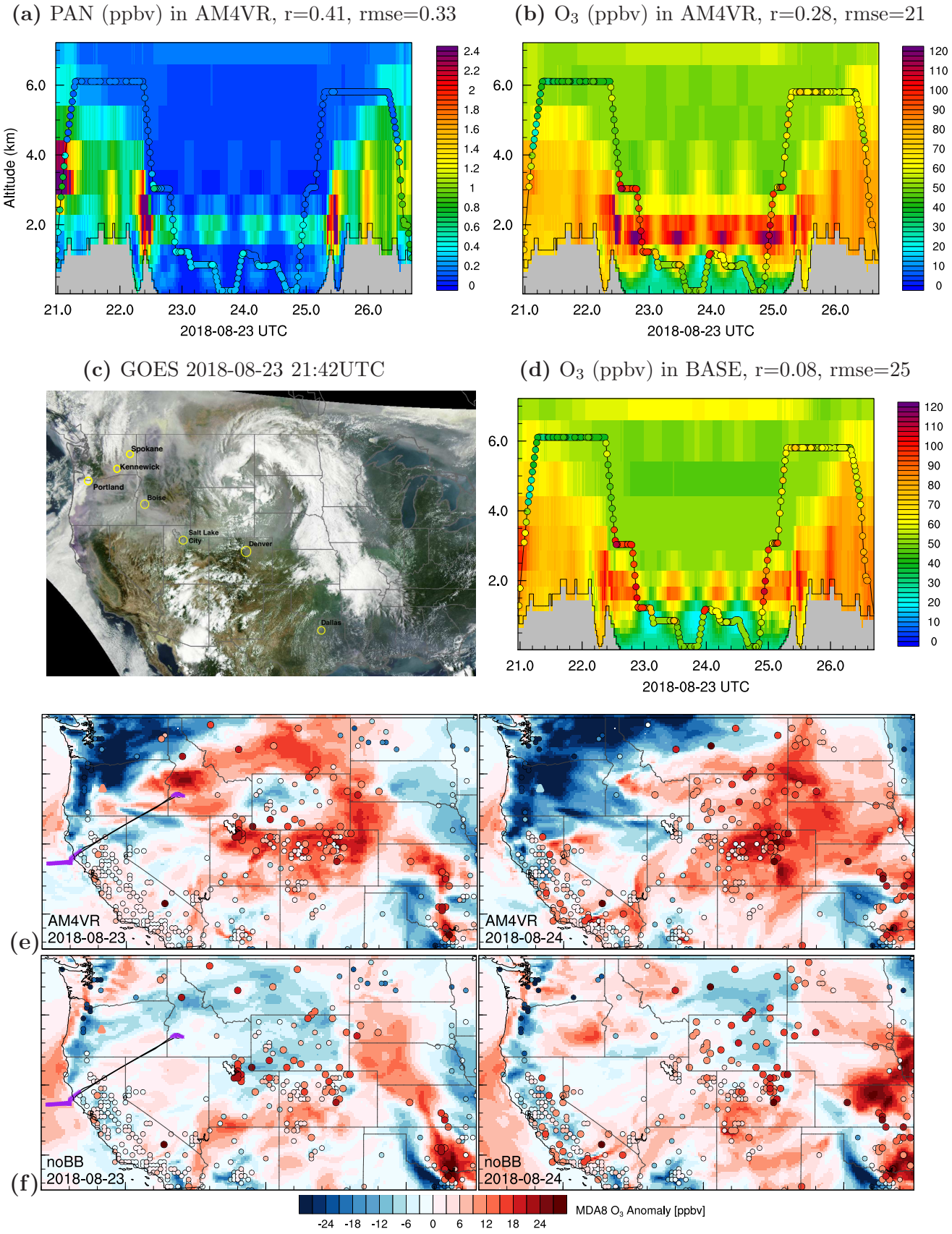

Figure 6. (a,b) Observed (filled circles) and AM4VR simulated PAN and O_3 for the August 23 flight; (c) GOES image; (d) Same as (b) but showing simulated O_3 from BASE. (e) Observed and AM4VR simulated surface MDA8 O_3 anomalies on August 23 and 24 (relative to August 22). (f) Same as (e) but showing noBB model results. The WE-CAN flight track is shown: purple crosses for below 4 km; black dots for above 4 km.